Studying physisorption processes and molecular friction of cycloparaphenylene molecules on graphene nano-sized flakes: role of $\pi\cdots\pi$ and CH$\cdots\pi$ interactions

A. Pérez-Guardiola, A. J. Pérez-Jiménez, and J. C. Sancho-García*

Departamento de Química Física,
Universidad de Alicante, E-03080 Alicante, Spain

May 26, 2017

*E-mail: jc.sancho@ua.es

Abstract

We theoretically study, by means of dispersion-corrected and cost-effective methods, the strength of non-covalent interactions between cyclic organic nanorings (i.e. [8]cycloparaphenylene molecule) and nano-sized (e.g. $C_{96}H_{24}$) graphene flakes acting as substrates. Both $CH\cdots\pi$ and $\pi\cdots\pi$ driven interactions are investigated, according to the relative orientation between the two weakly interacting monomers, whose potential energy profiles are accurately calculated in both cases. These configurations provide different physisorption curves, with the $CH\cdots\pi$ interaction leading to a larger well depth, and are found to slightly depend on edge effects of the nano-sized graphene flakes. Additionally, we fit the energy profiles to a compact (analytical) potential function, and study the atomic-scale friction between the molecule and the surface in the search of mechanisms for new molecular machines.

Key words: cycloparaphenylenes, graphene nanoflakes, physisorption processes, molecular friction, non-covalent interactions, DFT-D3/NL, HF-3c.

1 Introduction

Cyclic organic nanorings are emerging carbon nanoforms with many envisioned applications [1–5]. This family of molecules can be viewed as the cyclic analogues of linear conjugated oligomers, for instance [n]CycloParaPhenylenes ([n]CPPs, see Figure 1) are formed upon bending n phenylene units in *para* position until closing the corresponding nanoring, with their versatile, size-selective and gram-scale synthesis already achieved by a few groups [6–9] and for systems of variable size up to $n = 18$ units. Among those promising chemical functions, these organic nanorings might constitute ideal templates, or building blocks, for the controlled growth of uniform Single-Walled Carbon Nanotubes (SWCNTs) of defined diameter, according to the number of units of the molecules acting as precursors, or with pre-defined borders, armchair or zigzag, according to the nature of the oligomer to be employed [10]. However, despite some successful recent attempts in the search of new synthetic routes paving the way to the targeted SWCNTs, like the functionalization of [n]CPPs with fused Polycyclic Aromatic Hydrocarbons (PAHs) or with heteroarenes [11–14], some open questions about the detailed molecular mechanism and the optimal experimental conditions are still not fully resolved, and thus additional research is still needed before viable applications of these molecules for that ambitious goal materialize.

The crystalline structure of solid-state samples of [n]CPPs, in which quasi-onedimensional but disjoint nanochannels are known to coexist with the herringbone pattern typical of PAHs crystals [15], might help to understand and then further engineer possible synthetic routes fuelling the aforementioned synthesis. We have recently rationalized the energy stability for the complete set of self-assembled dimers found in the crystalline structure

of $[6-12]$CPPs, and how their different orientations could drive from a thermodynamical point of view (i.e. via their relative contribution to the cohesive energy) the formation of crystals depending on the system size [16]. This supramolecular order and morphology of the samples might facilitate the growing mechanism of SWCNTs, via some Diels-Alder mechanism with C_2H_4 or by some C_2H radical attacks, and subsequent dehydrogenation reactions [17, 18], which could benefit from immobilizing the samples on some substrates to induce a fully directional growth, an issue we would thus like to consistently explore here.

The aromatic surface of graphene [19, 20] makes it an ideal substrate for immobilization of these organic nanorings through $CH\cdots\pi$ and $\pi\cdots\pi$ non-covalent interactions. Graphene nano-sized flakes (or nanoislands on other substrates) are extremely useful models to study these highly local interactions in adsorption processes [21–23], as they can also be easily functionalized [24] and produced by STM experiments through mechanical contact between the tip and the surface or through electro-exfoliation [25]. Once a reasonable nano-sized graphene flake is selected one can choose the corresponding nanoring size to avoid pronounced edge effects. Actually, according to the two possible orientations of the $[n]$CPP molecular backbone with respect to the flat graphene-like surface, one can also study the strength and equilibrium distance of the $CH\cdots\pi$ and of the $\pi\cdots\pi$ involved non-covalent interactions, similarly to the driven interactions found between parallel-displaced (face-to-face) and T-shaped benzene-graphene models. These interactions can be characterized by the corresponding energy profile corresponding to the physisorption process, disclosing thus useful information and structure-property relationships for the creation of new supramolecular functional ma-

terials. Furthermore, investigating the rotation of the cyclic nanoring against the surface would also allow to characterize the corresponding energy profiles for this molecular friction.

Note that the aforementioned strategy demands the use of theoretical methods being both cost-effective, due to the size of the weakly bound systems to be tackled, as well as highly accurate, able to account for all the concurring electronic and/or dispersion interactions needed to disclose the routes for a fine-tuned use of [n]CPPs in substrate-mediated chemical processes. We will thus first present the set of Density Functional Theory (DFT) models selected for it, underlining the way in which the non-covalent interactions are safely introduced, before applying them to the calculation of well depths and distances for the physisorption processes tackled. We will also simultaneously explore if other recently developed low-cost methods (e.g. HF-3c) can accurately reproduce these results, paving thus the way towards extensions to larger systems and/or further molecular engineering studies.

2 Theoretical framework

The dispersion interactions are expected to become the strongest component of the physisorption energy profiles in these (non-polar) molecules. It is known that DFT might suffer from some drawbacks to incorporate these interactions in standard treatments, due to the semi-local nature of the exchange-correlation kernels used, and thus being unable to fully capture the long-range correlation acting between electrons situated at separated points $\mathbf{r}$ and $\mathbf{r}'$ in space. Therefore, we will rely on the D3(BJ) and NL methods (*vide infra*) coupled with the B3LYP exchange-correlation functional [26, 27]

to incorporate these effects both accurately and cost-effectively.

The former D3(BJ) method employs pair-wise interactions between all atoms, A and B, separated by the internuclear distance $R_{AB} = |R_A - R_B|$, as a function of the set of nth-order interatomic dispersion coefficients (C_n^{AB}) and a damping function $f_n = (a_1 R_{AB}^0 + a_2)^n$ to switch the energy from medium- to short-distances, with $R_{AB}^0 = \sqrt{\frac{C_8^{AB}}{C_6^{AB}}}$. The model is truncated at second order and it takes the final form [28, 29]:

$$E^{\mathrm{D3(BJ)}}(R_{AB}) = -\sum_{n=6,8} s_n \sum_{B>A}^{atom\ pairs} \frac{C_n^{AB}}{R_{AB}^n + f_n(R_{AB}^0)}, \tag{1}$$

with the s_n and a_i ($i = 1, 2$) the standard parameters fitted for the functional specifically selected [30–32]. This method is dubbed as B3LYP-D3(BJ) after appending the suffix of the dispersion correction to the original B3LYP model.

Another approach makes uses of a Non-Local (NL) kernel [33] with information from densities at both points in space, $\rho(\mathbf{r})$ and $\rho(\mathbf{r}')$, coupled through an interaction function $\Phi(\mathbf{r}, \mathbf{r}')$ with the correct asymptotic behaviour $|\mathbf{r} - \mathbf{r}'|^{-6}$:

$$E_c^{\mathrm{NL}}[\rho, \rho'] = \int d\mathbf{r} \rho(\mathbf{r}) \left[\frac{1}{2} \int d\mathbf{r}' \Phi(\mathbf{r}, \mathbf{r}', b, C) \rho(\mathbf{r}') + \beta(b) \right], \tag{2}$$

where the parameters b and C are also known for the functional selected [34]. This method is correspondingly named as B3LYP-NL, and it has been shown before to behave very accurately for all kind of weak chemical interactions [35, 36].

We finally benchmark the recently developed (low-cost) HF-3c method [37–39] in the sense that a minimal basis set is used, largely reducing the

final cost of a calculation, and with the appendix -3c meaning three pairwise corrections in the form:

$$E^{\mathrm{HF-3c}} = E_{\mathrm{HF/MINIX}} + E_{\mathrm{D3(BJ)}} + E^{gCP}_{\mathrm{BSSE}} + E_{cR_{AB}}, \tag{3}$$

where $E_{\mathrm{HF/MINIX}}$ is the Hartree-Fock (HF) energy with the MINIX basis set, $E_{\mathrm{D3(BJ)}}$ is merely a re-parameterized version of the D3(BJ) correction presented previously, E^{gCP}_{BSSE} denotes a geometrical counterpoise correction (gCP) to account for the expected Basis Sets Superposition Error (BSSE), and $E_{cR_{AB}}$ corrects the systematically overestimated covalent bond lengths (R_{AB}) for electronegative elements A and B. Despite its simplicity, the method has been shown before to reliably capture the main physics behind intermolecular interactions of [n]CPPs compounds [40].

2.1 Other technical details

We always employ adequate basis sets (i.e., cc-pVDZ for geometry optimizations and def2-TZVP for single-point energy calculations) and the release 3.0.3 of the ORCA package [41] including the corresponding auxiliary (def2-TZVP/JK) basis sets for the more demanding calculations after invoking the 'chain-of-spheres' (COSX) technique [42] to alleviate the associated computational cost. The numerical integration thresholds for both the exchange-correlation functional and the non-local, if any, correction were always strengthened with respect to the default values, to avoid any numerical limitation or noise for non-covalently bound complexes.

3 Results and discussion

3.1 Optimized monomers and built-in model for the weakly bound complexes

The computational protocol followed starts with the gas-phase optimization, at the B3LYP/cc-pVDZ level, of the monomers presented in Figure 2. The minima nature of the monomers was confirmed by all $(3N-6)$ positive frequencies obtained. These optimized structures are subsequently used for the rest of single-point energy calculations reported here. As a representative geometrical magnitude for assessing the reliability of the method used, we choose for the [8]CPP molecule ($C_{48}H_{32}$) the diameter defined as the distance between the opposite *ipso*-carbon atoms, being calculated here to be 11.1 Å compared with the experimental (X-ray) value of 10.9 Å [15], and the bond length of the benzenoid rings, calculated to be 1.405 Å compared again with the experimental value of 1.40 Å. Note also the inter-ring and alternating dihedral angles of 30.1° found between neighbouring benzene rings, in agreement with other studies [40].

Note that, to model the graphene nanoflakes, we employ the finite-sized molecules $C_{xx}H_{yy}$, with xx/yy being 54/18 and 96/24, also known as circumcoronene and circumcircumcoronene, respectively, with the size of the latter being large enough to correctly represent bulk effects, according to recent benchmark studies [43]. The use of finite molecular models, with the edges capped necessarily with H atoms, bring some advantages since they can be studied with a variety of highly performing theoretical methods, actually those developed for molecular systems and their nanoaggregates. The averaged optimized CC distances for $C_{54}H_{18}$ and $C_{96}H_{24}$ are 142.1 and 143.1 pm, respectively, compared with that of 142 pm for bulk graphene/graphite, and

thus within the expected uncertainty when comparing theoretical and experimental results [44]. More significant differences are found at the periphery rings, with CC distances ranging between 136.5 and 143.8 pm (137.4 and 144.9) for $C_{54}H_{18}$ ($C_{96}H_{24}$) due to pronounced edge effects. Actually, according to the relative sizes between the [8]CPP and both $C_{xx}H_{yy}$ monomers, we will also try to concomitantly investigate the influence, if any, of edge effects of the graphene nanoflakes on the physisorption process.

We then build a dimer in which we situate the origin of the coordinate system at the center of mass of the graphene nanoflake, with the z axis being normal to its surface, and with the center of mass of the [8]CPP molecule on top of it. The intermolecular distance R thus corresponds to that between the center of masses of both monomers, and is aligned correspondingly with the z axis. The association or interaction energies for the weakly bound complexes at all distances are calculated as $\Delta E(R) = E([8]\text{CPP}\cdots C_{xx}H_{yy}) - E([8]\text{CPP}) - E(C_{xx}H_{yy})$, in steps of $\Delta R = 0.2$ Å, except in the vicinity of the well depth for which ΔR is reduced to 0.05 Å. Note that: (i) the adsorption energies for benzene on graphene are fairly insensitive to the adsorption site [45]; and (ii) we also neglect herein the deformation energy, the energy change when the isolated monomers are forced to readapt their geometry to that optimal for the dimer; however, these induced geometrical changes in the monomers upon formation of weakly bound complexes are sufficiently small, actually 0.3 (0.4) kcal/mol for the [8]CPP ($C_{96}H_{24}$) monomers, and are thus not expected to affect the conclusions reached here.

3.2 Exploration of computational methods: the case of [8]CPP$\cdots$C$_{54}$H$_{18}$

We first present in Figure 3 the energy profiles for the interaction energy between the [8]CPP and the $C_{54}H_{18}$ graphene nanoflake, for both configurations dominated by CH$\cdots\pi$ and $\pi\cdots\pi$ interactions. The B3LYP-based curves, despite using the large def2-TZVP basis set, were further corrected by the CounterPoise (CP) method to take into account and thus correct any residual Basis Set Superposition Error (BSSE). We also extract from these energy profiles the distance R_e at which the well depth $\Delta E(R_e)$ takes its minimum energy, gathering the values consequently in Table 1. We can easily see, independently of the method employed, how for the CH$\cdots\pi$ interactions: (i) the energy values for $\Delta E(R_e)$ are twice as large than those computed for the $\pi\cdots\pi$ interactions, probably arising from the much larger surface contact between both monomers in this case [46]; and (ii) the interaction energy per ring, $\frac{\Delta E(R_e)}{n}$, is comprised between 3.8 and 4.1 kcal/mol. Furthermore, the distance for the $\pi\cdots\pi$ interaction lies in the expected range of $3.30-3.40$ Å, once one discounts half of the diameter (i.e. 11.1 Å) of the nanoring to the R_e distances contained in Table 1.

Keeping in mind the additivity nature of the non-covalent interactions, we also modelled within the B3LYP-D3(BJ), B3LYP-NL, and HF-3c methods, a simplified system in which the pristine $C_{54}H_{18}$ graphene nanoflake interacts with a unique benzene ring, with the plane formed by the C atoms of the latter residing either perpendicular (i.e. mimicking the CH$\cdots\pi$ interactions) or parallel (i.e. mimicking the $\pi\cdots\pi$ interactions) to the surface. First of all, we find well depth between -5.1 and -5.7 kcal/mol for the former case, which means an overestimation (i.e. more negative values) of around $24-28$ % with

respect to the $\frac{\Delta E(R_e)}{n}$ obtained before for the whole [8]CPP. In the case of $\pi\cdots\pi$ interactions, the well depth are comprising between -10.0 and -11.2 kcal/mol, and thus representing approximately 70 % of the interaction energies for the whole [8]CPP$\cdots C_{54}H_{18}$ complex. The R_e distances obtained for the $C_6H_6\cdots C_{54}H_{18}$ complex were found to differ only by 0.05 Å with respect to the previous cases. If we compare now with the $C_6H_6\cdots C_6H_6$ T-shaped and parallel displaced configurations, see for instance reference values at the CCSD(T)/aug-cc-pVQZ level from Ref. [47], we obtain higher values as it was expected from the larger number of pairwise non-local interactions.

3.3 Selection of the theoretical method

As regards the performance of the different methods assessed in the previous section, the HF-3c results are always close and comprised between those of B3LYP-D3(BJ) and B3LYP-NL, approaching in fact the latter but keeping an excellent trade-off between accuracy and computational cost. Due to the slight overestimation of interaction energies usually provided by the B3LYP-D3(BJ) method [48], which it has been shown to also happen for CH$\cdots\pi$ and $\pi\cdots\pi$ benzene-benzene interactions [49], and the quality of the B3LYP-NL method for a large variety of non-covalently bound systems [50], we will employ in the following the HF-3c method for dealing with the larger systems tackled along the rest of the study. Note that it would be possible to further decrease the computational cost by using a disperson-corrected semiempirical method (e.g. PM6-DH2) but it has also been shown that this leads to root-mean-squared errors of up to 1 kcal/mol in the case of benzene-benzene interactions in a set of benchmark systems [51]. Thus, taking into account all these facts, we select the HF-3c as the most reliable cost-effective

alternative to explore here the existing interactions between larger graphitic and cyclic carbon nanoforms.

3.4 Extending the size of graphene flakes: the cases of [8]CPP$\cdots$($C_{54}H_{18}$)$_2$ and [8]CPP$\cdots C_{96}H_{24}$

We will further consider if a second sheet of nano-sized graphene flakes, with the relative orientation between the stacked sheets as it is exactly found in graphite, would have any influence on the aforementioned values. Taking into account the relative strength of the CH$\cdots\pi$ and $\pi\cdots\pi$ interactions, we will exclusively focus on the former. Table 1 includes the new R_e and $\Delta E(R_e)$ values, which just differ by only $1-2$ % with respect to the values obtained before using only one sheet. This shows how the conclusions reached here will also hold for an infinite stack of nano-sized graphene sheets.

We now extend the 2D dimensions of the nano-sized graphene flake considered, going from $C_{54}H_{18}$ to $C_{96}H_{24}$, to disentangle the possible influence of edge effects on the previously calculated energy profiles. Note that the dimensions of the latter nano-sized graphene flake, 15.7x17.4 Å, are sufficiently large (compare the structures shown in Figures 3 and 4) to accommodate a [8]CPP molecule with a diameter of 11.1 Å . Table 1 shows how the R_e distances are not significantly modified in this case, although the interaction energies are stabilized by a considerable amount. Actually, the strength for the CH$\cdots\pi$ interactions is 2.5 times higher than that found for the $\pi\cdots\pi$ case, thus underlying the viability of some epitaxial nanochannel-like grotwh of the samples.

Actually, if we repeat the same exercise than before for the CH$\cdots\pi$ in-

teractions, that is, comparing the interaction energy per ring $\frac{\Delta E(R_e)}{n}$ of -5.3 kcal/mol with that for a single T-shaped benzene ring of -5.5 kcal/mol, we can see how these two values perfectly match now indicating much weaker edge effects in this case. This suggests an approximate linear relationship in the form $\Delta E(R_e)\,\{[n]\mathrm{CPP}\cdots\mathrm{C_{96}H_{24}}\} \approx n\Delta E(R_e)\,\{\mathrm{C_6H_6}\cdots\mathrm{C_{96}H_{24}}\}$. In the case of $\pi\cdots\pi$ interactions, we get a interaction energy for benzene with $\mathrm{C_{96}H_{24}}$ of -10.85 kcal/mol, to be compared with an experimental estimate of -11.5 kcal/mol for the interaction energy between benzene and infinite graphene [52], and thus showing again negligible edge effects, and a distance R_e of 3.35 Å, to be compared to that of 3.25 Å in the case of the whole [8]CPP molecule, the latter thus fully representative of the expected $\pi\cdots\pi$ nature of the interactions involved.

We finally explore the impact of estimating the repulsive three-body effects through the form approximated by [53]:

$$E^{\mathrm{D3(BJ)}}(R_{AB},R_{AC},R_{BC}) = \sum_{C>B>A}^{atom\ \ triples} C_9^{ABC}\frac{(3\cos\theta_{AB}\cos\theta_{BC}\cos\theta_{AC}+1)}{(R_{AB}R_{BC}R_{AC})^3} f_n(\overline{R}_{ABC}), \tag{4}$$

where C_9^{ABC} is the corresponding nth-order interatomic dispersion coefficient ($C_9^{ABC} \approx -\sqrt{C_6^{AB}C_6^{BC}C_6^{AC}}$) and θ_{IJ} are the internal angles of the triangle formed by the internuclear distances $R_{AB}-R_{BC}-R_{AC}$, with $\overline{R}_{ABC}$ the geometric mean of R_{AB}, R_{BC}, and R_{AC}, and $f_n(\overline{R}_{ABC})$ a damping function. This correction, when applied to the [8]CPP$\cdots\mathrm{C_{96}H_{24}}$ system, slightly shifts the physisorption curves and modifies the interaction energies given in Table 1 by only 4.1 and 1.9 kcal/mol, for the CH$\cdots\pi$ and $\pi\cdots\pi$ interactions, respectively, in line with previous findings for polycyclic conjugated hydrocarbons [54] and without significantly affecting the conclusions reached here.

3.5 Improved Lennard-Jones potential function

In classical force field expressions, the intermolecular forces are represented by an electrostatic and a Lennard-Jones (LJ) or similar term, with the latter relying usually on two parameters, the LJ radii and well depths. A correct description of condensed phases, soft matter, or interfacial phenomena needs often the reparameterization of this term for quantitative accuracy [55–57] before attempting to perform any reliable molecular dynamics simulation. However, although this simple model is able to reproduce the main features of non-covalent interactions around equilibrium distances, it might overestimate the short-range interactions, and thus possibly the shape of any energy profile for physisorption.

We will complementarily explore here the use of an Improved LJ (ILJ) potential function to express the physisorption profiles in a compact way, recently described in the literature and providing great accuracy for the pairwise atom-atom interactions of rare gas molecules in gas-phase [58]:

$$V(R) = \varepsilon \left[\frac{m}{n(R) - m} \left(\frac{R_e}{R} \right)^{n(R)} - \frac{n(R)}{n(R) - m} \left(\frac{R_e m}{R} \right)^{m} \right], \qquad (5)$$

with ε and R_e the depth of the potential well and the corresponding distance, $m = 6$ for neutral-neutral systems, and the $n(R)$ function given by:

$$n(R) = \beta + 4 \left(\frac{R}{R_e} \right)^2, \qquad (6)$$

introducing the β parameter as a measure of the hardness/softness of the interacting systems since $n(R \to 0) = \beta$. This $n(R)$ dependence is expected to lead to a correct behavior in a wide range of intermolecular distances. We collect in Table 2 the values of β obtained by a leasts-squares fitting of Eqs. (5)-(6) to the HF-3c curves, for the CH$\cdots\pi$ and $\pi\cdots\pi$ interactions and for

both nano-sized graphene flakes considered. The depth and location of the potential well is perfectly reproduced by the model, see Table 2, in agreement with previous studies of physisorption processes of small molecules on coronene [59]. Figure 4 shows the whole repulsive and long-range attractive regions, with the largest deviations occurring for the $\pi \cdots \pi$ stacking and restricted to the intermediate region between $4-7$ Å. We add the physisorption profiles obtained with the highly used UFF [60] and AMBER [61] force fields, with the G09 package [62] and assigning charges with the QEq method [63], to compare these results with the ILJ and the HF-3c expression. Note also that this ILJ expression has also been successfully applied to the energy ordering of nanoaggregates of up to 20-25 benzene molecules [64], thus showing a great potential for further applications within the field.

3.6 [8]CPP$\cdots$$C_{96}H_{24}$ friction studies

Finally, we would like to investigate how the molecular friction, depending generally speaking on the roughness and the chemistry of the surface, might impact on the dynamical evolution of the physisorption process. Note that only recently atomic-scale (STM and/or AFM) experiments are able to probe this highly directional effect [65, 66] and theoretical studies are still scarce. Furthermore, the interfacial energy for adsorbates sliding or rotating over a graphene-like surface is expected to complement the current understanding about the friction mechanism in pristine and functionalized graphene flakes [22], as well as to participate in the design of molecular machines and motors operating at the nanoscale [67].

We present in Figure 5 the effect of rotating the [8]CPP molecule against

the nano-sized ($C_{96}H_{24}$) graphene surface, again using the HF-3c method and in the range $\left[0, \frac{\pi}{2}\right]$. We explore both possibilities, either with the molecule frictioning the surface through the CH bonds (CH$\cdots\pi$ interactions) or through the twisted benzene rings closest to the surface ($\pi\cdots\pi$ interactions) and note that: (i) the symmetry point group of an idealized [8]CPP molecule is D_{8h}, and thus the range of angles explored should be sufficient to infer any periodicity effects although the effective symmetry of the system (molecule plus nanoflake) would probably decrease; and (ii) we keep a rigid and flat graphene surface and thus neglect the influence of any out-of-plane (flexural) elastic deformation.

For the case of CH$\cdots\pi$ interactions, the initial structure (shown in Figure 6) corresponds to the angle of minimum energy, with the H atoms pointing mostly to the inner part of the benzene, and thus maximizing the quadrupole-quadrupole interactions [68]. We indeed observe a periodic curve with an energy peak of 3.42 kcal/mol every $\frac{\pi}{6}$ approximately, indicating a low energy barrier of only a few times the value of $k_{\mathrm{B}}T$ at room temperature, and thus relatively easy to overcome as a function of temperature. Actually, for a value (T = 298K) of $k_{\mathrm{B}}T \approx 0.6$ kcal/mol, we can observe a range of angles around 10° freely available for rotating the molecule once it was physisorbed. Note that the rotation of organic molecules, like C_{60} or PCBM derivatives, at room temperature and in bulk phase, is known to contribute to the energetic disorder of the samples [69]. That peak of maximum energy corresponds to the relative orientation also displayed in Figure 6, where the rotation originates larger repulsive interactions. Similar findings are found for the $\pi\cdots\pi$ interactions, with a even lower energy barrier of 2.64 kcal/mol for fully rotating the molecule and a larger $\frac{\pi}{4}$ period between energy peaks, which allows a

deeper understanding of the molecular friction mechanisms and anticipates possible design path of molecular machines based on [n]CPP molecules.

4 Conclusions

We have theoretically studied the non-covalent interactions between the [8]CPP molecule, a phenylene oligomer with cyclic topology, and a pair of nano-sized graphene flakes of increasing size, involving CH$\cdots\pi$ and $\pi\cdots\pi$ stacking depending on how the [8]CPP approaches to the flat surface. The dispersion-corrected and cost-effective HF-3c method has revealed as a reliable and robust theoretical tool for this kind of studies. Interestingly, the strength of the CH$\cdots\pi$ binding is at least twice as high than the $\pi\cdots\pi$ stacking, which might be exploited for the controlled and highly directional layer-by-layer growth of the samples.

The locality of the weak interactions is analyzed by adding a second graphene-like sheet, with a negligible influence on the results. On the other hand, we have also disclosed the influence of edge effects, which may be sizable if the dimensions of the [n]CPP molecule are close to that of the nano-sized graphene flake. Nonetheless, extending the length and width of the nano-sized graphene flake have allowed us to bracket the interaction energy in the case of having more extended graphene surfaces. Complementarily, the additive effect of weak forces in the CH$\cdots\pi$ stacking is probed by modelling a simpler case, a benzene molecule instead of the [8]CPP system, to infer a linear relationship between the binding energy and the number of benzene rings, which is not so pronounced in the case of the $\pi\cdots\pi$ stacking since the adjacent bent rings play also some role.

Furthermore, we have fitted the obtained data to a physically meaningful potential functions (the ILJ model) for non-covalent interactions. We have also investigated the mechanical behavior of the [8]CPP system at the nanoscale inspecting the friction isotropy and its strength, obtaining low energy barriers for rotating the molecule once it is physisorbed. Overall, we hope the present study contributes to the understanding and quantification of adhesive forces and interfacial phenomena in carbon-based materials, allowing thus to further model interfacial phenomena and/or for the growth of $[n]$CPP samples once the first monolayer is immobilized by the graphitic-like substrate, stimulating more efforts in the challenging field of the use of cyclic nanorings as templates for the controlled growth of SWCNTs and their subsequent applications.

Acknowledgements

This work is supported by the "Ministerio de Economía y Competitividad" of Spain and the "European Regional Development Fund" through project CTQ2014-55073-P. We kindly acknowledge L. Muccioli (U. Bologna, Italy) for a critical reading of the manuscript.

References

[1] H. Omachi, Y. Segawa, K. Itami, Acc. Chem. Res. **45**, 1378 (2012).

[2] S. Yamago, E. Kayahara, T. Iwamoto, Chem. Rec. **14**, 84 (2014).

[3] M. R. Golder, R. Jasti, Acc. Chem. Res. **48**, 557 (2015).

[4] S. E. Lewis, Chem. Soc. Rev. **44**, 2221 (2015).

[5] Y. Segawa, A. Yagi, K. Matsui, K. Itami, Angew. Chem. Int. Ed. **55**, 5136 (2016).

[6] R. Jasti, J. Bhattacharjee, J. B. Neaton, C. R. Bertozzi, J. Am. Chem. Soc. **130**, 17646 (2008).

[7] H. Takaba, H. Omachi, Y. Yamamoto, J. Bouffard, K. Itami, Angew. Chem. Int. Ed. **48**, 6112 (2009).

[8] S. Yamago, Y. Watanabe, T. Iwamoto, Angew. Chem. Int. Ed. **49**, 757 (2010).

[9] E. Kayahara, V. K. Patel, J. Xia, R. Jasti, S. Yamago, Synlett **26**, 1615 (2015).

[10] H. Omachi, T. Nakayama, E. Takahashi, Y. Segawa, K. Itami, Nat. Chem. **5**, 572 (2013).

[11] T. J. Sisto, S. Tian X, R. Jasti, J. Org. Chem. **77**, 5857 (2012).

[12] T. Nishiuchi, X. Feng, V. Enkelmann, M. Wagner, K. Müllen, Chem. Eur. J. **18**, 16621 (2012).

[13] F. E. Golling, M. Quernheim, M. Wagner, T. Nishiuchi, K. Müllen, Angew. Chem. Int. Ed. **53**, 1525 (2014).

[14] F. E. Golling, S. Osella, M. Quernheim, M. Wagner, D. Beljonne, K. Müllen, Chem. Sci. **6**, 7072 (2015).

[15] J. Xia, R. Jasti, Angew. Chem. Int. Ed. **51**, 2474 (2012).

[16] M. Reche-Tamayo, M. Moral, A. J. Pérez-Jiménez, J. C. Sancho-García, J. Phys. Chem. C **120**, 22627 (2016).

[17] E. H. Fort, L. T. Scott, J. Mater. Chem. **21**, 1373 (2011).

[18] H.-B. Li, A. J. Page, S. Irle, K. Morokuma, J. Phys. Chem. Lett. **4**, 3176 (2013).

[19] A. H. Castro Neto, F. Guinea, N. M. R. Peres, K. S. Novoselov, A. Geim, Rev. Mod. Phys. **81** 109 (2009).

[20] A. K. Geim, Science **324**, 1530 (2009).

[21] P. Lazar, F. Karlický, P. Jurečka, M. Kocman, E. Otyepková, K. Šafářová, M. Otyepka, J. Am. Chem. Soc. **135**, 6372 (2013).

[22] M. Pykal, P. Jurečka, F. Karlický, M. Otyepka, Phys. Chem. Chem. Phys. **18**, 6351 (2016)

[23] E. Otyepková, P. Lazar, K. Cepe, O. Tomanec, M. Otyepka, Appl. Mat. Today **5**, 142 (2016).

[24] F. Karlicky, E. Otyepkova, R. Lo, M. Pitonak, P. Jurecka, M. Pykal, P. Hobza, M. Otyepka, J. Chem. Theory Comput. **2017**, 13, 1328.

[25] C. Rubio-Verdú, G. Sáenz-Arce, J. Martínez-Asencio, D. C. Milan, M. Moaied, J. J. Palacios, M. J. Caturla, C. Untiedt, Phys. Chem. Chem. Phys. **2017**, 19, 8061.

[26] A. D. Becke, J. Chem. Phys. **1993**, 98, 1372.

[27] V. Barone, C. Adamo, Chem. Phys. Lett. **1994**, 224, 432.

[28] S. Grimme, J. Antony, S. Ehrlich, H. Krieg, J. Chem. Phys. **2010**, 132, 154104.

[29] S. Grimme, S. Ehrlich, L. Goerigk, J. Comput. Chem. **2011**, 32, 1456.

[30] A. D. Becke, E. R. Johnson, J. Chem. Phys. **2005**, 122, 154101.

[31] E. R. Johnson, A. D. Becke, J. Chem. Phys. **2005**, 123, 024101.

[32] E. R. Johnson, A. D. Becke, J. Chem. Phys. **2006**, 124, 174104.

[33] O. A. Vydrov, T. Van Voorhis, J. Chem. Phys. **2010**, 133, 244103.

[34] W. Hujo, S. Grimme, J. Chem. Theory Comput. **2011**, 7, 3866.

[35] J. Aragó, E. Ortí, J. C. Sancho-García, J. Chem. Theory Comput. **2013**, 9, 3437.

[36] J. Calbo, E. Ortí, J. C. Sancho-García, J. Aragó, Ann. Rep. Comput. Chem. **2015**, 11, 37.

[37] R. Sure, S. Grimme, J. Comput. Chem. **2013**, 34, 1672.

[38] L. Goerigk, C. A. Collyer, J. R. Reimers, J. Phys. Chem. B **2014**, 118, 14612.

[39] J. G. Brandenburg, S. Grimme, Top. Curr. Chem. **2014**, 345, 1.

[40] J. V. Climent-Medina, A. J. Pérez-Jiménez, M. Moral, E. San-Fabián, J. C. Sancho-García, ChemPhysChem **2015**, 16, 1520.

[41] F. Neese, WIREs Comput. Mol. Sci. **2012**, 2, 73.

[42] F. Neese, F. Wennmohs, A. Hansen, U. Becker, Chem. Phys. **2009**, 356, 98.

[43] S. Grimme, C. Mück-Lichtenfeld, J. Antony, J. Phys. Chem. C **2007**, 111, 11199.

[44] E. Brémond, M. Savarese, N. Q. Su, Á. J. Pérez-Jiménez, X. Xu, J. C. Sancho-García, C. Adamo, J. Chem. Theory Comput. **2016**, 12, 459.

[45] P.-P. Zhou, R.-Q. Zhang, Phys. Chem. Chem. Phys. **2015**, 17, 12185.

[46] K. Yuan, R.-S. Zhao, J.-J. Zheng, H. Zheng, S. Nagase, S.-D. Zhao, Y.-Z. Liu, X. Zhao, J. Comput. Chem. **2017**, DOI:10.0002/jcc.24.743.

[47] M. O. Sinnokrot, C. D. Sherrill, J. Phys. Chem. A **2006**, 110, 10656.

[48] S. T. Schneebeli, A. D. Bochevarov, R. A. Friesner, J. Chem. Theory Comput. **2011**, 7, 658.

[49] K. Strutyński, M. Melle-Franco, J. A. N. F. Gomes, J. Phys. Chem. A **2013**, 117, 2844.

[50] L. Goerigk, J. Chem. Theory Comput. **2014**, 10, 968.

[51] K. Strutyński, J. A. N. F. Gomes, M. Melle-Franco, J. Phys. Chem. A **2013**, 118, 9561.

[52] R. Zacharia, H.Ulbricht, T. Hertel, Phys. Rev. B **2004**, 69, 155406.

[53] O. A. von Lilienfeld, A. Tkatchenko, J. Chem. Phys. **2013**, 132, 234109.

[54] J. C. Sancho-García, A. J. Pérez-Jiménez, Y. Olivier, J. Chem. Phys. **2015**, 142, 054702.

[55] O. A. von Lilienfeld, D. Andrienko, J. Chem. Phys. **2006**, 124, 054307.

[56] L. Muccioli, G. D'Avino, R. Berardi, S. Orlandi, A. Pizzirusso, M. Ricci, O. M. Roscioni, C. Zannoni, Top. Curr. Chem. **2014**, 352, 39.

[57] M. Moral, W.-J. Son, J. C. Sancho-Garca, Y. Olivier, L. Muccioli, J. Chem. Theory Comput. **2015**, 11, 3383.

[58] F. Pirani, S. Brizi, L. F. Roncaratti, P. Casavecchia, D. Cappelletti, F. Vecchiocattivi, Phys. Chem. Chem. Phys. **2008**, 10, 5489.

[59] Md. B. Yeamin, N. Faginas-Lago, M. Alberti, I. G. Cuesta, J. Sánchez-Marín, A. M. J. Sánchez de Merás, RSC Adv. **2014**, 4, 54447.

[60] A. K. Rappé, C. J. Casewit, K. S. Colwell, W. A. Goddard III, W. M. Skiff, J. Am. Chem. Soc. **1992**, 114, 10024.

[61] W. D. Cornell, P. Cieplak, C. I. Bayly, I. R. Gould, K. M. Merz Jr., D. M. Ferguson, D. C. Spellmeyer, T. Fox, J. W. Caldwell, P. A. Kollman, J. Am. Chem. Soc. **1995**, 117, 5179.

[62] Gaussian 09, Revision D.03, M. J. Frisch, G. W. Trucks, H. B. Schlegel, G. E. Scuseria, M. A. Robb, J. R. Cheeseman, G. Scalmani, V. Barone, B. Mennucci, G. A. Petersson, H. Nakatsuji, M. Caricato, X. Li, H. P. Hratchian, A. F. Izmaylov, J. Bloino, G. Zheng, J. L. Sonnenberg, M. Hada, M. Ehara, K. Toyota, R. Fukuda, J. Hasegawa, M. Ishida, T. Nakajima, Y. Honda, O. Kitao, H. Nakai, T. Vreven, J. A. Montgomery, Jr., J. E. Peralta, F. Ogliaro, M. Bearpark, J. J. Heyd, E. Brothers, K. N. Kudin, V. N. Staroverov, R. Kobayashi, J. Normand, K. Raghavachari, A. Rendell, J. C. Burant, S. S. Iyengar, J. Tomasi, M. Cossi, N. Rega, J. M. Millam, M. Klene, J. E. Knox, J. B. Cross, V. Bakken, C. Adamo, J. Jaramillo, R. Gomperts, R. E. Stratmann, O. Yazyev, A. J. Austin, R. Cammi, C. Pomelli, J. W. Ochterski, R. L. Martin, K. Morokuma, V. G. Zakrzewski, G. A. Voth, P. Salvador, J. J. Dannenberg, S. Dapprich,

A. D. Daniels, Ö. Farkas, J. B. Foresman, J. V. Ortiz, J. Cioslowski, and D. J. Fox, Gaussian, Inc., Wallingford CT, 2009.

[63] A. K. Rappé, L. M. Bormann-Rochotte, D. C. Wiser, J. R. Hart, M. A. Pietsch, C. J. Casewit, W. M. Skiff, Mol. Phys. **2007**, 105, 301.

[64] M. Bartolomei, F. Pirani, J. M. C. Marques, J. Comput. Chem. **2015**, 36, 2291.

[65] A. J. Weymouth, D. Meuer, P. Mutombo, T. Wutscher, M. Ondracek, P. Jelinek, F. J. Giessibl, Phys. Rev. Lett. **2013**, 111, 126103.

[66] C. M. Almeida, R. Prioli, B. Fragneaud, L. G. Cançado, R. Paupitz, D. S. Galvao, M. De Cicco, M. G. Menezes, C. A. Achete, R. B. Capaz, Sci. Rep. **2016**, 6, 31569.

[67] W. R. Browne, B. L. Feringa, Nature Nanotech. **2006**, 1, 25.

[68] C. R. Martínez, B. L. Iverson, Chem. Sci. **2012**, 3, 2191.

[69] G. D'Avino, Y. Olivier, L. Muccioli, D. Beljonne, J. Mater. Chem. C **2016**, 4, 3747.

- **Table 1.** Interaction energies (kcal/mol) and distances (Å) for the minimum energy configuration of [8]CPP and $C_{xx}H_{yy}$ complexes.

- **Table 2.** Interaction energies (kcal/mol), distances (Å), and values of β for the minimum energy configuration of [8]CPP and $C_{xx}H_{yy}$ complexes, as calculated with the ILJ potential fitted for the HF-3c energy curves.

Table 1:

		CH$\cdots\pi$		$\pi\cdots\pi$	
Complex	Method	R_e	$\Delta E(R_e)$	R_e	$\Delta E(R_e)$
[8]CPP$\cdots$$C_{54}H_{18}$	B3LYP-D3(BJ)	4.75	-32.85	8.85	-15.45
	B3LYP-NL	4.80	-30.04	8.90	-14.69
	HF-3c	4.70	-32.42	8.80	-14.83
[8]CPP$\cdots$$(C_{54}H_{18})_2$	HF-3c	4.75	-32.94	–	–
[8]CPP$\cdots$$C_{96}H_{24}$	HF-3c	4.65	-42.59	8.75	-17.11

Table 2:

	CH$\cdots\pi$			$\pi\cdots\pi$		
Complex	β	R_e	$\Delta E(R_e)$	β	R_e	$\Delta E(R_e)$
[8]CPP$\cdots$C$_{54}$H$_{18}$	9.6333	4.70	-32.42	32.5856	8.80	-14.83
[8]CPP$\cdots$C$_{96}$H$_{24}$	9.5626	4.65	-43.11	29.7393	8.75	-17.11

- **Figure 1.** Chemical structure of the [n]CPP compounds.

- **Figure 2.** Top: Chemical structure of the [8]CPP oligomer; with the C atoms of the repeating unit along the backbone dark grey coloured. Middle and bottom: Chemical structure of the $C_{54}H_{18}$ and $C_{96}H_{24}$ compounds, respectively, used as a finite models for graphene nanoflakes.

- **Figure 3.** Interaction energy of the weakly bound [8]CPP$\cdots$$C_{54}H_{18}$ complex as a function of the intermolecular (center-of-masses) distance, for both CH$\cdots\pi$ (top) and $\pi\cdots\pi$ (bottom) configurations and with the B3LYP-D3(BJ), B3LYP-NL, and HF-3c methods. The structures shown correspond to the minimum energy (at R_e) situation.

- **Figure 4.** Interaction energy of the weakly bound [8]CPP$\cdots$$C_{96}H_{24}$ complex as a function of the intermolecular (center-of-masses) distance, for both CH$\cdots\pi$ (top) and $\pi\cdots\pi$ (bottom) configurations, and with the HF-3c nethod, the ILJ potential, and the AMBER and UFF force fields. The structures shown correspond to the minimum energy (at R_e) situation.

- **Figure 5.** Interaction energy for the rotation of the weakly bound [8]CPP $\cdots$ $C_{96}H_{24}$ complex, as calculated at the HF-3c level, for both CH$\cdots\pi$ (top) and $\pi\cdots\pi$ (bottom) configurations.

- **Figure 6.** Chemical structure (top view) of the weakly bound [8]CPP$\cdots$$C_{96}H_{24}$ complex at 0 (top) and $\frac{\pi}{4}$ (bottom) rotating angles along the z-axis perpendicular to the surface.

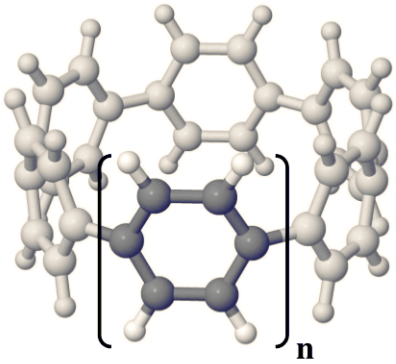

Figure 1.

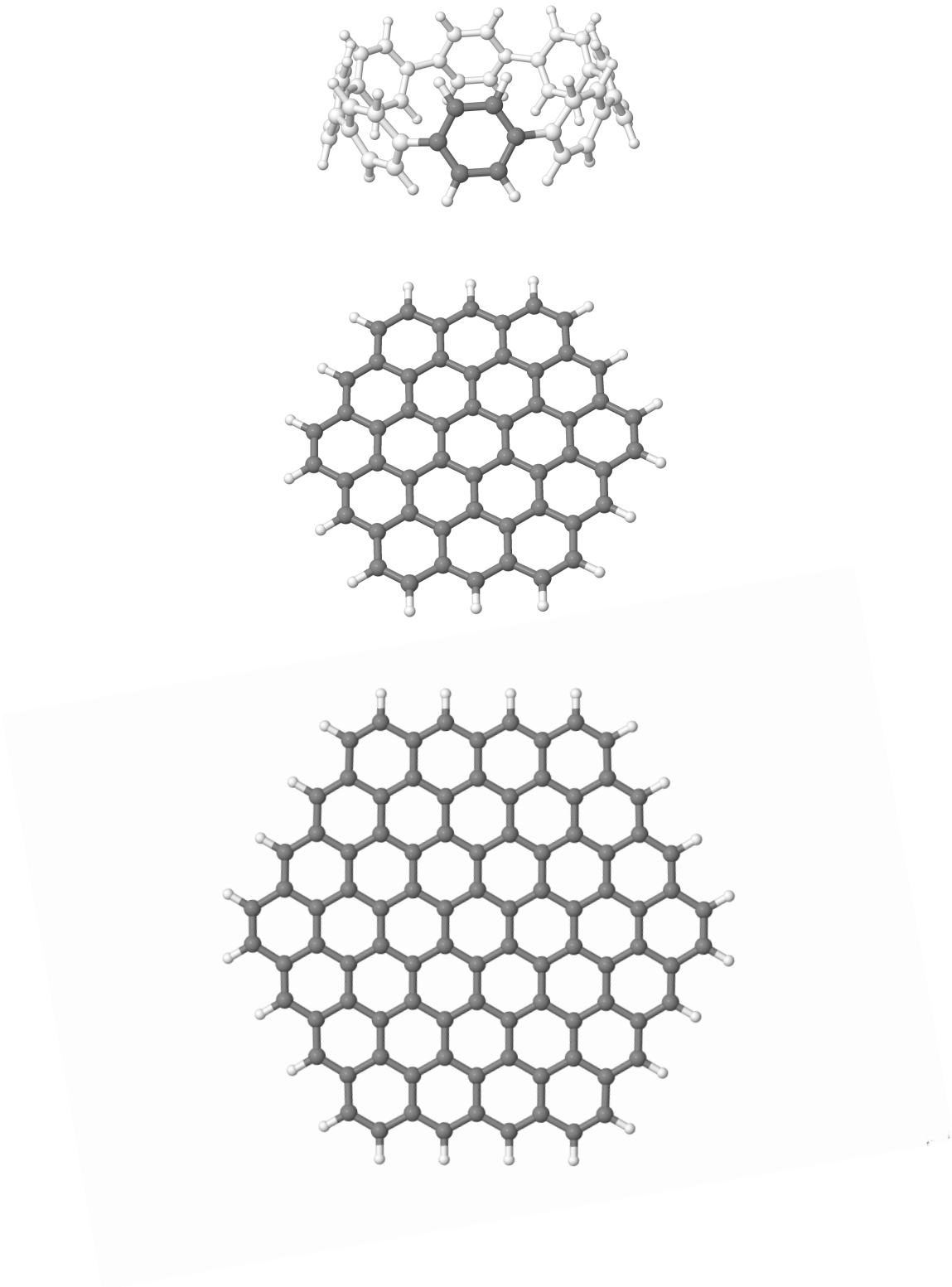

Figure 2.

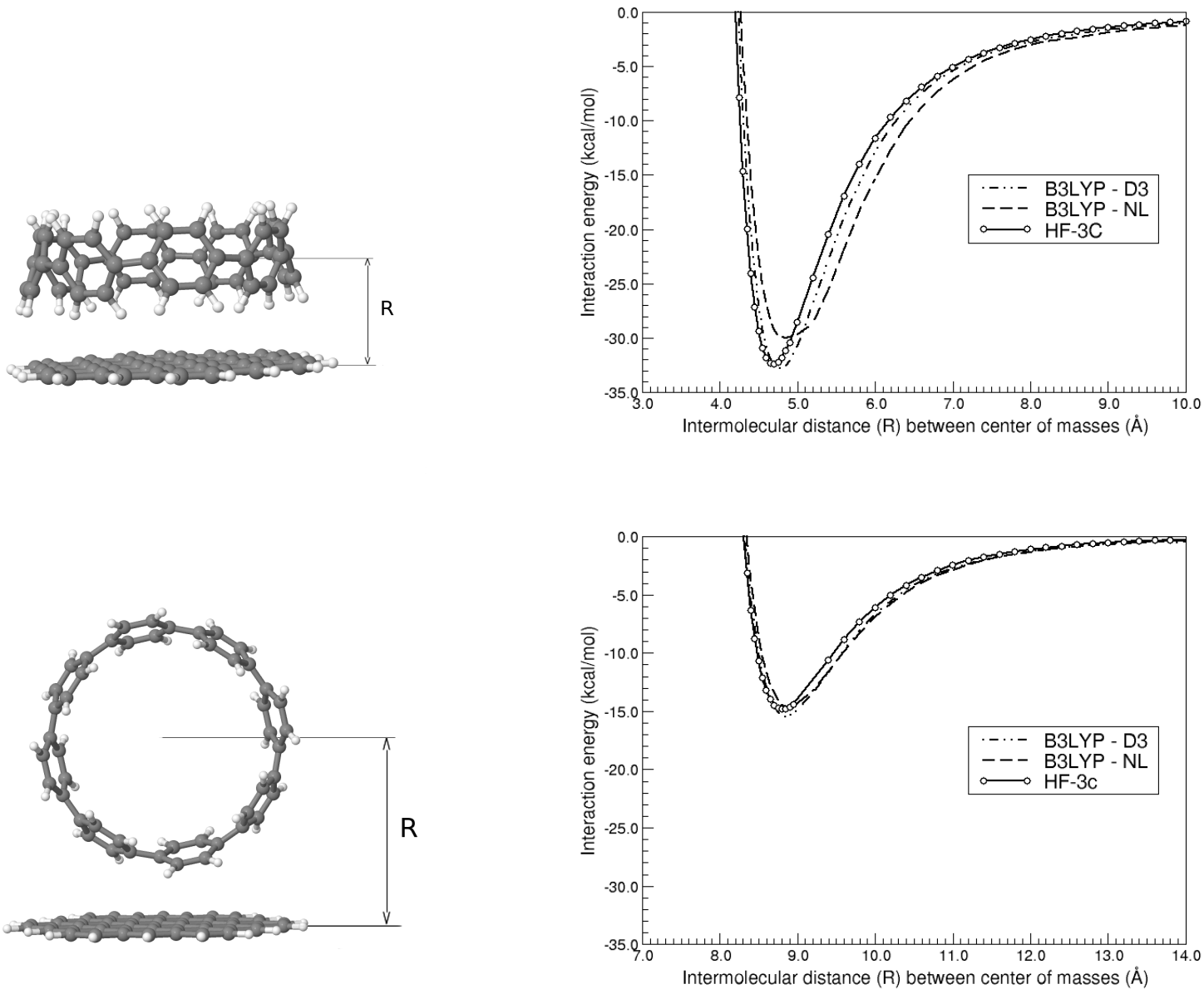
R
R
Interaction energy (kcal/mol)
Intermolecular distance (R) between center of masses (Å)
B3LYP - D3
B3LYP - NL
HF-3C
Interaction energy (kcal/mol)
Intermolecular distance (R) between center of masses (Å)
B3LYP - D3
B3LYP - NL
HF-3c

Figure 3.

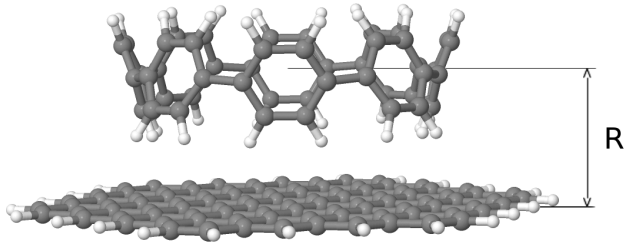
R

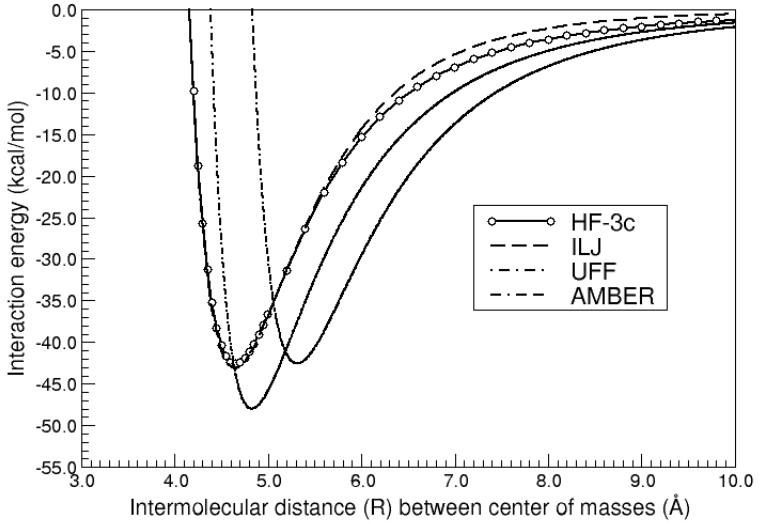
Interaction energy (kcal/mol)
0.0
-5.0
-10.0
-15.0
-20.0
-25.0
-30.0
-35.0
-40.0
-45.0
-50.0
-55.0
3.0
4.0
5.0
6.0
7.0
8.0
9.0
10.0
Intermolecular distance (R) between center of masses (Å)
HF-3c
ILJ
UFF
AMBER

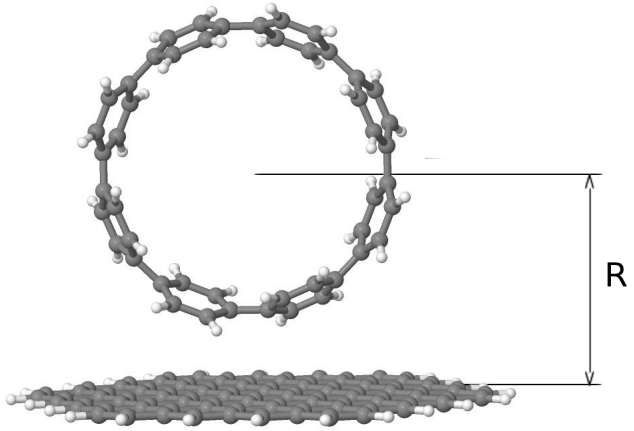
R

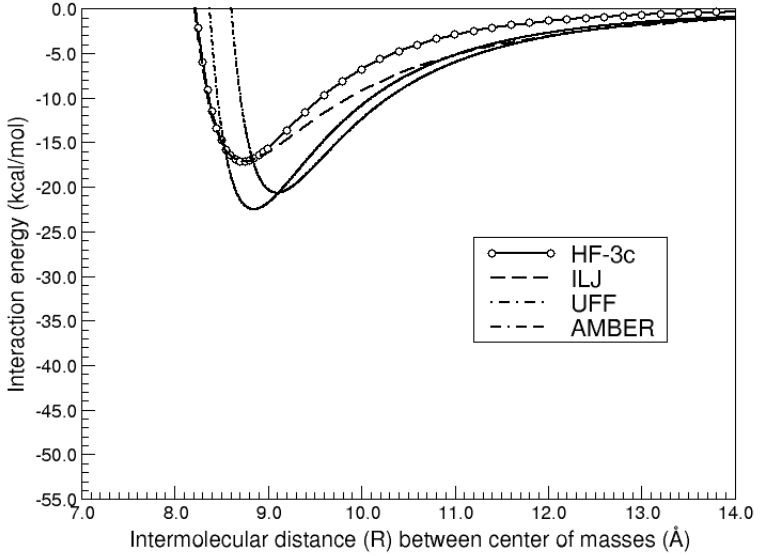
Interaction energy (kcal/mol)
0.0
-5.0
-10.0
-15.0
-20.0
-25.0
-30.0
-35.0
-40.0
-45.0
-50.0
-55.0
7.0
8.0
9.0
10.0
11.0
12.0
13.0
14.0
Intermolecular distance (R) between center of masses (Å)
HF-3c
ILJ
UFF
AMBER

Figure 4.

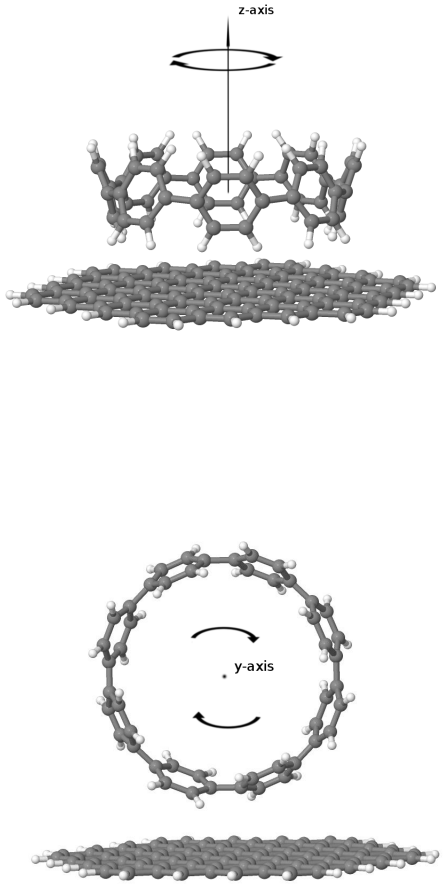
z-axis
y-axis
Jmol

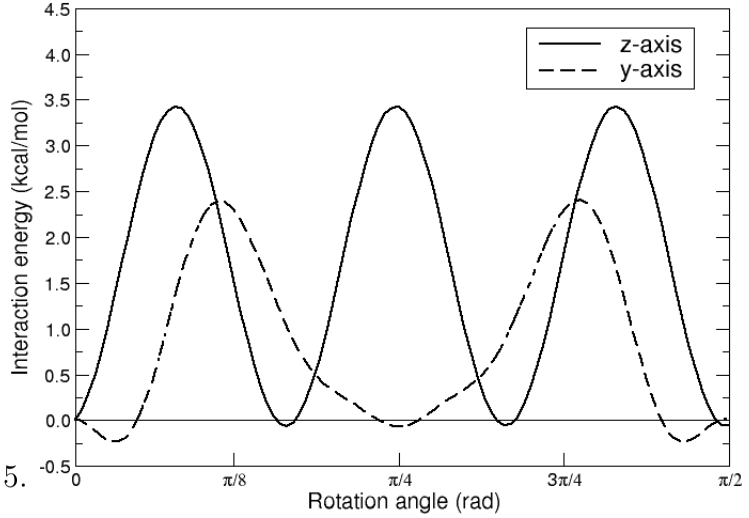
z-axis
y-axis
Interaction energy (kcal/mol)
Rotation angle (rad)
4.5
4.0
3.5
3.0
2.5
2.0
1.5
1.0
0.5
0.0
-0.5
0
π/8
π/4
3π/4
π/2

Figure 5.

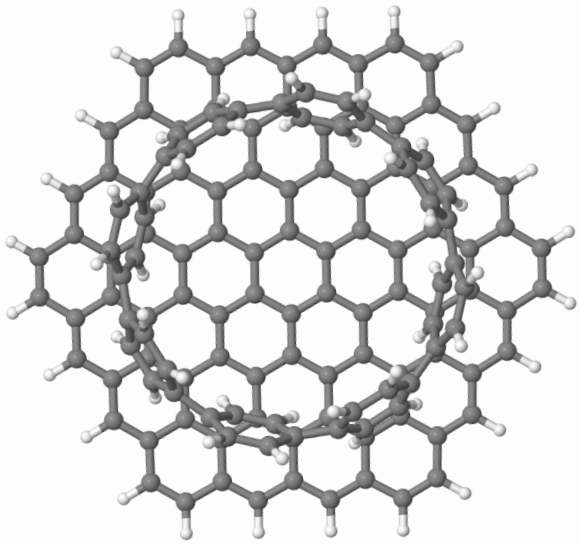

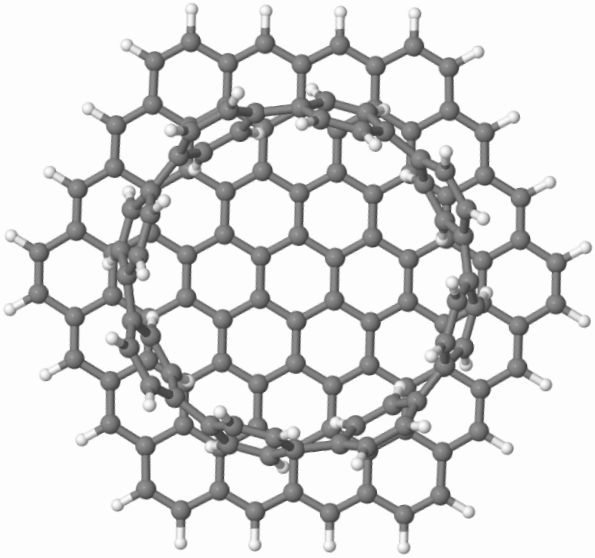

Figure 6.